

Chandra and *XMM-Newton* observations of the low-luminosity X-ray pulsators SAX J1324.4–6200 and SAX J1452.8–5949

Ramanpreet Kaur^{1*}, Rudy Wijnands², Alessandro Patruno², Vincenzo Testa³, GianLuca Israel³, Nathalie Degenaar², Biswajit Paul⁴, Brijesh Kumar¹

¹ *Aryabhata Research Institute of observational sciences, Manora Peak, Naini Tal, 263 129, India*

² *Astronomical Institute "Anton Pannekoek", University of Amsterdam, Kruislaan 403, 1098 SJ, Amsterdam, The Netherlands*

³ *INAF - Osservatorio Astronomico di Roma, via Frascati 33, 00040 Monte Porzio Catone, Italy*

⁴ *Raman Research Institute, C. V. Raman Avenue, Sadashivanagar, Bangalore 560 080, India.*

ABSTRACT

We present results from our *Chandra* and *XMM-Newton* observations of two low-luminosity X-ray pulsators SAX J1324.4–6200 and SAX J1452.8–5949 which have spin-periods of 172 s and 437 s respectively. The *XMM-Newton* spectra for both sources can be fitted well with a simple power-law model of photon index ~ 1.0 . A black-body model can equally well fit the spectra with a temperature of ~ 2 keV for both sources. During our *XMM-Newton* observations, SAX J1324.4–6200 is detected with coherent X-ray pulsations at a period of 172.86 ± 0.02 s while no pulsations with a pulse fraction greater than 15 % (at 98% confidence level) are detected in SAX J1452.8–5949. The spin period of SAX J1324.4–6200 is found to be increasing on a time-scale of $\dot{P} = (6.34 \pm 0.08) \times 10^{-9}$ s s⁻¹ which would suggest that the accretor is a neutron star and not a white dwarf. Using sub-arcsec spatial resolution of the *Chandra* telescope, possible counterparts are seen for both sources in the near-infrared images obtained with the SOFI instrument on the *New Technology Telescope*. The X-ray and near-infrared properties of SAX J1324.4–6200 suggest it to be either a persistent high mass accreting X-ray pulsar or a symbiotic X-ray binary pulsar at a distance ≤ 9 kpc. We identify the infrared counterpart of SAX J1452.8–5949 to be a late-type main sequence star at a distance ≤ 10 kpc, thus ruling out SAX J1452.8–5949 to be a high mass X-ray binary. However with the present X-ray and near-infrared observations, we cannot make any further conclusive conclusion about the nature of SAX J1452.8–5949.

Key words: binaries: close - pulsars: individual (SAX J1324.4–6200, SAX J1452.8–5949) - stars: neutron - X-rays: binaries

1 INTRODUCTION

In the past ten years, using the Advanced Satellite for Cosmology and Astrophysics (*ASCA*), *BeppoSAX* and the Rossi X-ray Timing Explorer (*RXTE*) satellites, a population of faint ($L_X \lesssim 10^{36}$ erg s⁻¹) X-ray sources has been found in our Galaxy which harbor a slow pulsating source with periods ranging from several seconds to over a thousand seconds. These ‘slow’ pulsators are found to harbor a variety of source types like anomalous X-ray pulsars (isolated slowly rotating neutron stars; e.g. Torii et al. 1998), accreting magnetized white dwarfs (i.e. intermediate polars, AM Her type systems; e.g., Misaki et al. 1996), and neutron stars accreting from a high-mass companion star (i.e., mostly as Be/X-ray

transients; e.g., Hulleman et al. 1998). Despite the successes in determining the nature of these slow pulsators, there remains a group of persistent systems whose nature still has not been determined. The X-ray properties of these sources suggest that most of them are neutron stars accreting from a high mass companion star, however accreting white dwarf cannot be excluded. Furthermore, in some cases, the possibility of a system in which a neutron star accretes from a low-mass companion star also cannot be excluded (Lin et al. 2002). More observations at all wavelengths (i.e., X-ray or near IR) could help to unveil the nature of these pulsators. In this paper, we present the results from our *Chandra*, *XMM-Newton* and *New Technology Telescope* (NTT) observations of two faint X-ray pulsators SAX J1324.4–6200 ($l = 306^\circ.79$, $b = 0^\circ.60$) and SAX J1452.8–5949 ($l = 317^\circ.65$, $b = -0^\circ.46$).

* E-mail: raman@aries.ernet.in

SAX J1324.4–6200 (hereafter SAX13), which has a

pulse period of ~ 170 s, was discovered serendipitously from observations of the low mass X-ray binary (LMXB) XB 1323–619 performed on August 22, 1997 with *BeppoSAX* (Angelini et al. 1998). The X-ray (1.8–10 keV) spectrum of the source could be fitted with either an absorbed power-law with photon index of 1.0 ± 0.4 and hydrogen column density, N_{H} of $7.8^{+2.7}_{-1.1} \times 10^{22} \text{ cm}^{-2}$ or with a black-body model with a temperature, kT of 2.4 ± 0.4 keV and N_{H} of $4^{+3}_{-2} \times 10^{22} \text{ cm}^{-2}$ (Angelini et al. 1998). SAX13 was also detected in the observations performed on XB 1323–619 using *ASCA* on August 4, 1994 (Angelini et al. 1998). In addition, pointed *ASCA* observations (of 187 ks) were performed on SAX13 on February 2, 2000 and the source was detected with a pulse period of ~ 171.2 s (Lin et al. 2002). Lin et al. (2002) found a possible orbital period of the system of 27 ± 1 hour and suggested that the system could be a LMXB pulsar. Recently, during short observations performed using *Swift* on December 30, 2007, SAX13 was detected with a pulse period of 172.8 s (Mereghetti et al. 2008) which would imply a spin down over the last 10 years of $\dot{P} \sim 6 \times 10^{-9} \text{ s s}^{-1}$. Mereghetti et al. (2008) identified a possible 2MASS near-infrared counterpart in the *Swift* error circle of SAX13 with a K band magnitude of 14.39 ± 0.08 and suggested that the source could be a persistent Be accreting X-ray pulsar.

SAX J1452.8–5949 (hereafter SAX14) was discovered using *BeppoSAX* with a spin period of ~ 437 s (Oosterbroek et al. 1999). The X-ray spectra of the source could be fitted well with an absorbed power-law model with a photon index of 1.4 ± 0.6 . Oosterbroek et al. (1999) suggested that SAX14 could be an accreting Be X-ray pulsar at a distance of 6–12 kpc with the luminosity of $\sim 10^{34} \text{ erg s}^{-1}$.

2 X-RAY OBSERVATIONS

Our X-ray observations of SAX13 and SAX14 were carried out using the European Photon Imaging Camera (EPIC) aboard the *XMM-Newton* satellite and advanced CCD Imaging Spectrometer (ACIS) aboard the *Chandra* satellite.

2.1 *XMM-Newton*

SAX13 and SAX14 were observed for ~ 19 ks on January 11, 2008 (Obs ID. 0511010201) and ~ 7 ks on February 7, 2008 (Obs ID. 0511010501) respectively. Both the EPIC-MOS and EPIC-*pn* cameras (Turner et al. 2001; Struder et al. 2001) were operated in the *Full Frame* mode and with the medium filter. The observation details are summarized in Table 1. The EPIC observation data files were processed using the *XMM-Science Analysis System* (SAS version 7.1.0)¹. Investigation of the full-field count-rate of SAX13 revealed ~ 3 ks of high-count rate background particle flaring and is removed from the data. However we did not see any significant background flaring in SAX14 observation. We used the task *edetect_chain* to find the exact position of X-ray source in the combined images of EPIC-MOS and EPIC-*pn* instruments. In the *BeppoSAX* error circle of SAX13 (Angelini et al. 1998), we detected only one source in the *XMM-Newton* observations at a position of R.A. = $13^{\text{h}} 24^{\text{m}} 26^{\text{s}}.64$

and DEC. = $-62^{\circ} 01' 18''.48$ with an error circle of radius $2''.0$ (90% confidence; J2000; all coordinates in the paper are for J2000 epoch). In the *BeppoSAX* error circle of SAX14 (Oosterbroek et al. 1999), only one source is detected in the *XMM-Newton* observations at a position of R.A. = $14^{\text{h}} 52^{\text{m}} 52^{\text{s}}.80$ and DEC. = $-59^{\circ} 49' 08''.04$ with an error circle of radius $2''.0$ (90% confidence). The error circle on the position of X-ray source is adopted as a quadratic sum of the bore sight error of the *XMM-Newton* telescope² and the statistical error given by the task *edetect_chain*.

2.2 *Chandra*

SAX13 and SAX14 were observed for ~ 1 ks each on November 28, 2007 (Obs ID. 9012) and December 30, 2007 (Obs ID. 9014) respectively. The details of the observations are given in Table 1. The data was obtained with the ACIS-I CCDs operating in the FAINT mode for both sources. We processed the event 2 files using the standard software packages CIAO 4.0³ and CALDB 3.4.2⁴. The task *wavdetect* was used to find the exact position of X-ray source in the image. One source is detected in the *XMM-Newton* error circle of SAX13 with a total of 87 counts at a position of R.A. = $13^{\text{h}} 24^{\text{m}} 26^{\text{s}}.70$ and DEC. = $-62^{\circ} 01' 19''.49$ with the error circle of radius $0''.65$ (Figure 1). In the *Chandra* image of SAX14, one source is detected (Figure 2) in the *XMM-Newton* error circle of SAX14, albeit with only 4 counts at a position of R.A. = $14^{\text{h}} 52^{\text{m}} 52^{\text{s}}.70$ and DEC. = $-59^{\circ} 49' 8''.07$ with the error circle of radius $0''.95$. The average background count is ~ 1 count for a similar area in the full *Chandra* image of SAX14, indicates that indeed we have detected SAX14. The errors on the positions of SAX13 and SAX14 are obtained as a quadratic sum of the bore sight error of the *Chandra* telescope⁵, $1\text{-}\sigma$ *wavdetect* errors and a contribution that depends on the number of detected counts (van den Berg et al. 2004; especially important for SAX14).

3 INFRARED OBSERVATIONS AND DATA ANALYSIS

Near-infrared observations in the J , H , K_s wavebands were performed in February 2001 with the 3.58 m ESO-NTT telescope equipped with the near-infrared imager and spectrograph SOFI. The instrument was set up in large imaging mode with a pixel scale of $0''.29$ and a field of view of $5'.0 \times 5'.0$ when SAX13 was observed and in small imaging mode with a pixel scale of $0''.14$ and a field of view of $2'.5 \times 2'.5$ when SAX14 was observed (both in double ‘correlated’ readout mode). In both cases, the seeing conditions were very good, ranging from $0''.58$ to $0''.66$ between K_s and J bands. Images were acquired with the auto-jitter sequence, obtaining several dithered frames for each filter, that were then re-aligned and co-added together. Table 2 summarizes the observations. The acquisition mode is the usual

² See <http://xmm2.esac.esa.int/docs/documents/CAL-TN-0018.pdf>

³ *Chandra* Interactive Analysis of Observations (CIAO), <http://cxc.harvard.edu/ciao/>.

⁴ *Chandra* Calibration Database (CALDB), <http://cxc.harvard.edu/caldb/>

⁵ See <http://cxc.harvard.edu/cal/ASPECT/celmon>.

¹ See <http://xmm2.esac.esa.int/sas/>

Table 1. Log of the X-ray observations of SAX J1324.4–6200 and SAX J1452.8–5949.

Object	Telescope/Instrument	Date (UT)	ObsId	Total Observation Span (ks)
SAX J1324.4–6200	<i>Chandra</i> /ACIS-I	28 Nov 2007	9012	1.1
SAX J1452.8–5949	<i>Chandra</i> /ACIS-I	30 Dec 2007	9014	1.0
SAX J1324.4–6200	<i>XMM-Newton</i> /EPIC	11 Jan 2008	0511010201	19.3
SAX J1452.8–5949	<i>XMM-Newton</i> /EPIC	07 Feb 2008	0511010501	6.9

one for near-IR arrays: a number of single frames (NDIT) having exposure times of DIT (Detector Integrator Time) seconds are acquired and then co-added aboard generating an output image having exposure time equal to one DIT, but the signal-to-noise (S/N) statistics of NDIT×DIT seconds. All the output frames (Nframes) are then processed and co-added offline, generating the final science image.

Images were reduced using the package *eclipse* developed by ESO to handle near-IR observations. The pipeline executes the following steps: first, a master ‘sky’ images is obtained by median stacking all the frames for one observation and for each filter. This ‘sky’ image is subtracted to every single image generating sky-subtracted frames. This step also subtracts bias and dark current contributions. The images are then flat-fielded with flat field images obtained on the dome. In the case of SOFI, also a ‘screen’ correction image applied to correct for residual illumination gradients in the dome. At the end, the pre-reduced images are aligned and average stacked, with a proper σ -clipping selection, obtaining the science-ready final images. Source detection and photometry has been performed with the *daophot* package within IRAF¹. In particular, a second-order variable PSF model has been computed for our images to minimize positional biases due to the (small) PSF variation over the field. The output magnitudes have been aperture corrected and calibrated with the 2MASS catalog (Skrutskie et al. 2006). The same 2MASS has been used also to obtain an astrometric calibrations of the frames. The interactive software Skycat-GAIA has been used, selecting the portion of catalog of the area and fitting a solution to the image. The positions obtained in this way have (absolute) uncertainties of about 0.2, and relative uncertainties far below a fraction of a pixel.

As can be seen in the K_s image taken with NTT, the position of three point sources labeled as ‘C1’, ‘C2’, ‘C3’ are consistent with the *XMM-Newton* error circle of SAX13 (Figure 1). The position of two point sources labeled as ‘S1’ and ‘S2’ are consistent with the *XMM-Newton* error circle of SAX14 (Figure 2). The *Chandra* error circle for both the sources is also shown : the position of star ‘C1’ falls in the *Chandra* error circle of SAX13 and that of ‘S1’ in the *Chandra* error circle of SAX14. Therefore we consider ‘C1’ as the near-infrared counterpart of SAX13 and ‘S1’ of SAX14. We have listed the positions (in Right Ascension and Declination) and magnitudes in J , H , K_s bands for the near-infrared counterparts of SAX13 and SAX14 in Table 3. For the sake

of completeness, the positions and magnitudes of the other stars falling in the *XMM-Newton* error circles of SAX13 and SAX14 are also listed in Table 3.

4 DATA ANALYSIS AND RESULTS

4.1 Timing Analysis

The *XMM-Newton* EPIC-*pn* data were used for the timing analysis for both SAX13 and SAX14. The X-ray events were extracted in a circular region of radius 15” and 30” for SAX13 and SAX14, respectively, centered on the position of the target in the EPIC-*pn* image. We were forced to take smaller circular region for SAX13 as it was located close to a CCD gap. The background X-ray events were extracted with a similar circular region on the same CCD in a source-free region. The times of the events were transformed to barycentric times using the *SAS* tool *barycor* using the *Chandra* position of the source and the JPL-DE405 ephemeris. The events were re-binned with a time resolution of 0.2 s and the light curves were corrected for background contamination.

We reduced ≈ 16 ks of pointed observations from the EPIC-*pn* CCD camera for SAX13 and detected the source with a background corrected count rate of 0.28 counts s^{-1} . We folded the background corrected light curve in five chunks of ≈ 3000 s, with the best spin-period available from Mereghetti et al. (2008). The pulse profiles were then cross correlated with a template profile obtained by folding the entire light curve. The cross correlation returns the time of arrivals (TOAs) of each pulse profile with the fiducial point for the measurement fixed to be the peak of the template profile. The technique applied to measure the TOAs and their statistical uncertainties closely resemble the radio pulsar technique (e.g., Taylor 1992). The TOAs were then phase connected with a linear polynomial fit of the pulse phase to obtain the pulsar spin period. The measure of a spin period derivative using a phase coherent technique is prevented given the short baseline of the observation for which the phase-connected solution could be applied. Our measured spin period is $P_s = 172.86 \pm 0.02$ s (referred at MJD 54460; The error is calculated with 68% confidence level) and is consistent with the previous measurements of Mereghetti et al. (2008) that reported a spin period of 172.84 ± 0.1 s at MJD 54464.2. The phase-connected solution has not the precision required for an extrapolation to the previous observations of the source (see Table 5). Therefore we fitted all the previous and our new measured value of the spin period (Angelini et al. 1998, Lin et al. 2002, Mereghetti et al. 2008) with a linear relation $P_s(t) = P_0 + \dot{P}_s t$, where \dot{P}_s is the spin period derivative of the pulsar and P_0 is the spin period at the time $t = 0$. The value obtained from our fit

¹ Image Reduction and Analysis Facility (IRAF) is distributed by the National Optical Astronomy Observatories, which are operated by the Association of Universities for Research in Astronomy, Inc., under cooperative agreement with the National Science Foundation.

Table 2. Log of the 3.58 m ESO-NTT near-infrared observations of SAX J1324.4–6200 and SAX J1452.8–5949. N-DIT represents the Number of single frames, having exposure times of DIT (Detector Integrator Time) seconds and are used to generate an output image having exposure time equal to one DIT. The number of output frames are represented by Nframes.

Source	Date (UT)	<i>J</i>			<i>H</i>			<i>K_s</i>			FWHM(arcsec)
		DIT	NDIT	Nframes	DIT	NDIT	Nframes	DIT	NDIT	Nframes	
SAXJ1324.4–6200	06 Feb 2001	3	5	8	3	5	8	3	5	12	0.6
SAXJ1452.8–5949	08 Feb 2001	3	5	10	3	5	12	3	5	16	0.6

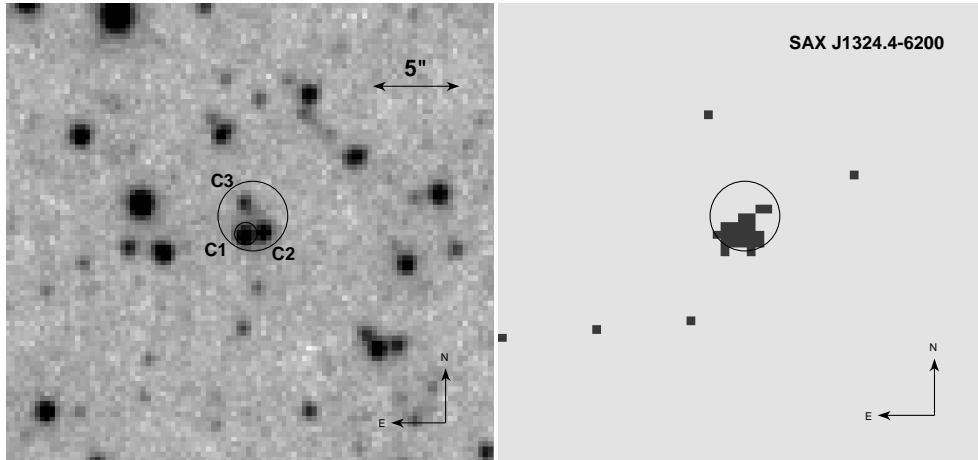


Figure 1. *Left* : The K_s waveband image of SAX J1324.4–6200 taken by SOFI instrument on the New Technology Telescope. The *XMM-Newton* error circle of radius $2''$ and the *Chandra* error circle of radius $0.65''$ of SAX J1324.4–6200 are also plotted. *Right* : *Chandra* ACIS-I image of SAX J1324.4–6200 with the *XMM-Newton* error circle of radius $2''$.

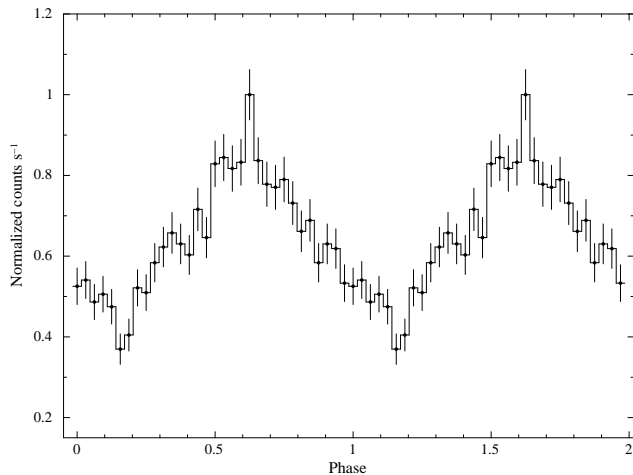


Figure 3. The *XMM-Newton* EPIC-*pn* 0.2–12 keV background subtracted pulse profile of SAX J1324.4–6200. Two cycles are shown for clarity.

is $\dot{P}_s = (6.34 \pm 0.08) \times 10^{-9} \text{ s s}^{-1}$ with a χ^2 of 4.46 for 3 degrees of freedom. The background subtracted pulse profile of SAX13 in the energy range 0.2 - 12 keV is shown in Figure 3.

We also folded the entire *XMM-Newton* light curve in one single profile to increase the S/N and measure the harmonic content and the fractional amplitude of the pulsation. The pulse profile is fitted well with a single sinusoid with a significance larger than 20σ and has a fractional amplitude of $(52 \pm 4)\%$.

SAX14 was detected with a background subtracted count rate of $0.05 \text{ counts s}^{-1}$. We repeated the same procedure (described above) for SAX14 using the best available spin period (Oosterbroek et al. 1999). However no significant pulse profiles have been detected in the energy band 0.2 - 12 keV with an upper limit on the pulsed fraction amplitude (Vaughan et al. 1994) of 15 % (at 98% confidence level). To further investigate the presence of pulsations, we divided the EPIC-*pn* light curve into soft (0.2 - 4 keV) and hard (4 - 12 keV) energy bands with equal count rate. No significant pulse profiles were detected in both soft and hard energy bands with an upper limit on the pulse fractional amplitude of 18% and 22% (at 98% confidence level) respectively.

4.2 Spectral Analysis

The *XMM-Newton* EPIC-*MOS* and *pn* data are used for spectral analysis for SAX13 and SAX14. We used the same extraction region for EPIC-*pn* data as were used for the timing analysis reported in §4.1 while a $30''$ circular region is used to extract the X-ray counts in the EPIC-*MOS* images for both sources. SAS tool *xmmselect* was used to extract both source and background spectra. We used *XSPEC* (version 11.0.0) for our spectral analysis. The resulting spectra were re-binned to have minimum of 20 counts per bin.

We fitted both power-law and black-body models to the SAX13 EPIC-*MOS* and *pn* X-ray spectra together. Both models could fit the data with a reduced χ^2 of ~ 1.0 for 385 degrees of freedom (dof). The full values of obtained fit parameters are given in Table 4. For the power-law model, the spectrum could be fitted with a photon index of 1.0 and

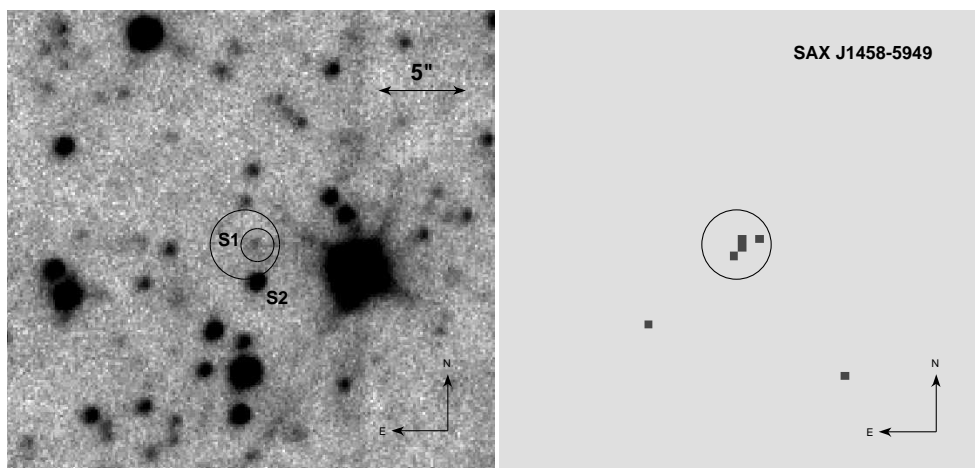


Figure 2. *Left* : The K_s waveband image of SAX J1452.8–5949 taken by SOFI instrument on the New Technology Telescope. The *XMM-Newton* error circle of radius $2''$ and the *Chandra* error circle of radius $0.65''$ of SAX J1452.8–5949 are also plotted. *Right* : *Chandra* ACIS-I image of SAX J1452.8–5949 with the *XMM-Newton* error circle of radius $2''$.

Table 3. J , H and K_s magnitudes of stars falling in the *XMM-Newton* error circle of SAX J1324.4–6200 and SAX J1452.8–5949. The stars listed here are also marked in the near-infrared ESO-NTT images shown in Figure 1 and 2.

Star	R.A. hh:mm:ss	DEC. ° ' "	J magnitude	H magnitude	K_s magnitude
Stars in <i>XMM-Newton</i> error circle of SAX J1324.4–6200					
C1	13:24:26.71	–62:01:19.59	19.57 ± 0.11	16.61 ± 0.09	14.97 ± 0.11
C2	13:24:26.56	–62:02:19.38	18.76 ± 0.10	16.48 ± 0.09	15.45 ± 0.11
C3	13:24:26.72	–62:01:17.71	18.37 ± 0.10	17.00 ± 0.09	16.62 ± 0.12
Stars in <i>XMM-Newton</i> error circle of SAX J1452.8–5949					
S1	14:52:52.72	–59:49:07.92	18.59 ± 0.12	17.75 ± 0.12	17.93 ± 0.12
S2	14:52:52.70	–59:49:10.14	16.92 ± 0.11	15.50 ± 0.10	15.06 ± 0.10

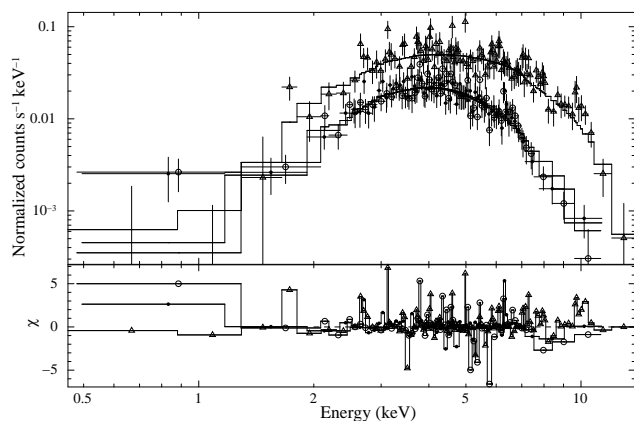


Figure 4. The *XMM-Newton* EPIC-MOS and *pn* spectra of SAX J1324.4–6200 fitted with an absorbed power-law model. The *pn* data points are represented by open triangles, the *MOS1* data points are represented by open circles and the *MOS2* data points are represented by filled circle.

an N_H of $5.8 \times 10^{22} \text{ cm}^{-2}$ while using a black-body model, we obtained a $kT = 2.2 \text{ keV}$ and an N_H of $3.1 \times 10^{22} \text{ cm}^{-2}$. The observed flux for both models in the 2 - 10 keV energy band is $\sim 5 \times 10^{-12} \text{ erg s}^{-1} \text{ cm}^{-2}$. With the present data, we

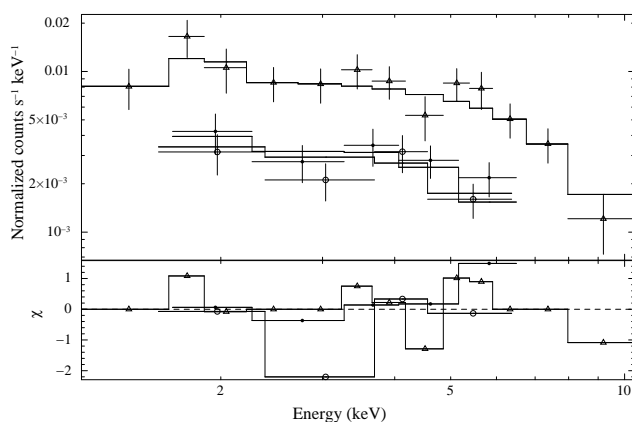


Figure 5. The *XMM-Newton* EPIC-MOS and *pn* spectra of SAX J1452.8–5949 fitted with an absorbed power-law model. The *pn* data points are represented by open triangles, the *MOS1* data points are represented by open circles and *MOS2* are represented by filled circle.

are unable to distinguish between the power-law and black-body model fit. The power-law fit to SAX13 *XMM-Newton* EPIC-MOS and *pn* spectra is shown in Figure 4. No sig-

Table 4. Spectral Parameters for SAX J1324.4-6200 and SAX J1452.8-5949 for *XMM-Newton* EPIC observations.

	SAX J1324.4-6200	SAX J1452.8-5949
Parameter	Spectral parameters of model (Absorption + power-law)	
$N_H \times 10^{22}$ (cm $^{-2}$)	5.81 ± 0.65	1.22 ± 0.69
Photon Index	1.01 ± 0.14	0.83 ± 0.28
Reduced χ^2 /dof	0.95/383	0.6/19
Observed Flux 2 - 10 keV (ergs cm $^{-2}$ s $^{-1}$)	$(4.5 \pm 1.3) \times 10^{-12}$	$(5.4 \pm 2.5) \times 10^{-13}$
Unabsorbed Flux 2 - 10 keV (ergs cm $^{-2}$ s $^{-1}$)	$(6.0 \pm 1.4) \times 10^{-12}$	$(5.8 \pm 2.9) \times 10^{-13}$
Parameter	Spectral parameters of model (Absorption + black-body)	
$N_H \times 10^{22}$ (cm $^{-2}$)	3.07 ± 0.42	< 0.54 (90% confidence)
Blackbody temperature (keV)	2.24 ± 0.14	1.82 ± 0.24
Reduced χ^2 /dof	1.0/383	0.7/20
Observed Flux 2 - 10 keV (ergs cm $^{-2}$ s $^{-1}$)	$(4.4 \pm 0.2) \times 10^{-12}$	$(4.9 \pm 0.4) \times 10^{-13}$
Unabsorbed Flux 2 - 10 keV (ergs cm $^{-2}$ s $^{-1}$)	$(5.0 \pm 0.3) \times 10^{-12}$	$(5.0 \pm 0.4) \times 10^{-13}$

nificant Fe 6.4 keV emission line is seen in the combined *XMM-Newton* EPIC-*MOS* and *pn* spectrum of SAX13 (Fig 4). To find an upper limit on Fe 6.4 keV emission line, we fixed the line-center at 6.4 keV in the spectrum and fitted a Gaussian to the line. The upper limit on the equivalent width of the 6.4 keV emission line is determined to be 118 eV (90% confidence limit).

Similarly, we fitted both power-law and black-body models to the SAX14 spectra. Both models provide acceptable fits with reduced χ^2 in the range of 0.6 - 0.7 for 20 dof. From the power-law model, we obtained a photon index, Γ of 0.8 and an N_H of 1.2×10^{22} cm $^{-2}$ (shown in Figure 5) while using the black-body model we obtained a kT = 1.8 keV and an $N_H = 0.5 \times 10^{22}$ cm $^{-2}$. The observed flux in 2 - 10 keV energy band (for both the models) is $\sim 5 \times 10^{-13}$ erg s $^{-1}$ cm $^{-2}$. The spectral parameters of SAX14 are listed in Table 4. No significant Fe 6.4 keV emission line is seen in the SAX14 spectra (Fig 5). However, an upper limit on iron 6.4 keV emission line in the combined *XMM-Newton* EPIC - *MOS* and *pn* spectrum of SAX14 is 436 eV (at 90% confidence level).

5 DISCUSSION

We carried out observations with the *Chandra* and *XMM-Newton* satellites to investigate the nature of the accreting X-ray pulsators SAX J1324.4-6200 and SAX J1452.8-5949. In addition, we obtained near-infrared data using the ESO-NTT to search for infrared counterparts for these pulsators.

5.1 SAX J1324.4-6200

During our *XMM-Newton* observation, SAX13 is detected with a pulse period of 172.85 ± 0.02 s, consistent with the pulse period obtained by Mereghetti et al. (2008) from observations made by *Swift* on December 30, 2007, just 10 days before our *XMM-Newton* observations. The spin period history of SAX13 clearly shows a linear increase in pulse period from 170.35 to 172.86 s over the last 14 years (Table 5) with spin period derivative $\dot{P} = (6.34 \pm 0.08) \times 10^{-9}$ s s $^{-1}$. The spin period of high mass X-ray binary (HMXB)

pulsars range from a few seconds to a few hundred seconds and display several spin-up/down trends on time-scales ranging from days to years (Bildsten et al. 1997). For example, 4U 1907+09, a persistent supergiant X-ray binary with $P_s = 440$ s, is spinning down for more than 15 years with $\dot{P} = 7.3 \times 10^{-7}$ s s $^{-1}$ (Baykal et al. 2001). Among LMXB pulsars, GX 1+4 has the longest spin period of ~ 141 s. LMXB pulsars show a wide range of spin-period derivatives ranging from $\sim 10^{-8}$ to $\sim 10^{-11}$ s s $^{-1}$ (Ferrigno et al. 2007; Chakrabarty et al. 1997). Intermediate Polars (IPs) are also slow pulsators with spin-period of few hundred seconds and usually show spin up phases with a typical spin period derivative $\sim -7 \times 10^{-11}$ s s $^{-1}$ (Patterson 1994). However there are a very few IPs which are found to be spinning down and the fastest spinning down intermediate polar PQ Gem is observed with $\dot{P} = 1.1 \times 10^{-10}$ s s $^{-1}$ (Mason 1997).

The measured spin torque can be used as a clue on the nature of the compact accretor in SAX13. The usual expression for the accretion torque on a compact accretor is : $I\dot{\omega} = \dot{M}\sqrt{0.5GM}r_A$ (Lipunov 1992), where I and $\dot{\omega}$ is the moment of inertia and the spin torque of the compact accretor respectively, M and \dot{M} is the mass and the mass accretion rate of the compact accretor respectively, r_A is the Alfvén radius and G is the Gravitational constant. r_A for a compact accretor is $\propto \mu^{4/7} M^{-1/7} \dot{M}^{-2/7}$, where μ is the magnetic moment of it. Thus the external torque applied from the accretion disk onto the compact object scales as $\propto M^{-3/7} R^{12/7} B^{2/7}$, where $B (= \mu R^3)$ is the magnetic field of the compact object and for a given X-ray luminosity, the value of \dot{M} is $\propto \frac{R}{M}$. The value of M , R and B can be fixed for a typical white dwarf in an intermediate polar and an accreting neutron star. Thus, given a certain observed X-ray luminosity, the ratio of a spin torque for a white dwarf and a neutron star would be :

$$\frac{\dot{\omega}_{wd}}{\dot{\omega}_{ns}} = \frac{M_{wd}^{-3/7} R_{wd}^{12/7} B_{wd}^{2/7}}{I_{wd}} \times \frac{I_{ns}}{M_{ns}^{-3/7} R_{ns}^{12/7} B_{ns}^{2/7}} \quad (1)$$

where the subscript ‘wd’ and ‘ns’ refer to white dwarf and neutron star respectively. A white dwarf has a moment of inertia $\approx 4 - 5$ order of magnitude larger than a neutron star. For the typical parameters of white dwarf and neutron star : $R_{wd} = 10^4$ km, $B_{wd} = 10^5$ G and $M_{wd} = 0.1M_\odot$; $R_{ns} = 10$ km, $B_{ns} = 10^8$ G and $M_{ns} = 1.4M_\odot$, the ratio between the expected accretion torques for the two com-

compact objects is $\approx 0.1 - 1$, implies that we cannot distinguish between a white dwarf and a neutron star system on the basis of the spin torque. However, for a high magnetic field neutron star ($B \approx 10^{12}$ G) the ratio between the expected accretion torques for the two compact objects is $\approx 10^{-2}$ which implies that a high B field neutron star system has a spin torque two orders of magnitude larger than a white dwarf. Since in SAX13, the observed spin down is comparable with measures of spin torques made for high B field accreting neutron stars, the presence of a neutron star is favored, unless the accretor is an intermediate polar with a high B field and a quite small mass.

The *XMM-Newton* spectra of SAX13 fits well with both power-law and black-body models. The spectral parameters of SAX13 (Table 4) are typical of an accreting neutron star X-ray pulsar with a high magnetic field. Accreting X-ray pulsars with low magnetic field strength usually display soft X-ray spectra with photon index ≥ 2.0 (Bildsten et al. 1997). IPs display hard X-ray spectra similar to high mass X-ray binary pulsars but they also show a strong iron $K\alpha$ emission line (e.g., Norton et al. 1991, Munro et al. 2004). The absence of Fe $K\alpha$ emission line in the SAX13 X-ray spectra further makes it very unlikely to be an IP.

With the *Swift* spatial resolution, Mereghetti et al. (2008) identified the possible infrared counterpart of SAX13 in the 2MASS K_S band image with magnitude 14.39 ± 0.08 . Figure 1 shows the ESO-NTT K_S band image of SAX13, zoomed-in at the position of SAX13. As can be seen, the single 2MASS star is resolved into three stars ‘C1’, ‘C2’ and ‘C3’ in an NTT K_S band image. The position of star ‘C1’ is consistent with the *Chandra* error circle of SAX13, and therefore ‘C1’ is the most likely near-infrared counterpart of SAX13.

Using the observed $N_H = 5.8 \times 10^{22} \text{ cm}^{-2}$ (Table 4), and the relation $A_V/N_H = 5.6 \times 10^{-22} \text{ mag cm}^2$ (Predehl et al. 1995), the corresponding A_V for SAX13 is calculated to be 32.54 mag. Using the above A_V , we calculated the near-infrared extinction in J , H and K_s waveband to be 9.01, 5.56 and 3.77 mag (Fitzpatrick 1999). Finally, the dereddened magnitudes of SAX13 are found to be $J = 10.56 \pm 0.11$ mag, $H = 11.05 \pm 0.09$ mag and $K = 11.20 \pm 0.11$ mag. Here, we do not take into account the uncertainties in the A_V . Also, we don’t deny that a part of the X-ray absorption density could be local to the X-ray source, and not necessarily apply to the companion star.

With the above extinction-free J , H and K_s magnitudes of SAX13, we used a black-body model to estimate the distance to different type of stars (main-sequence stars, supergiants and giants), for a given temperature and a radius (Cox 2000). With these calculations, we found that any late-type main sequence star (M through A type) would lie at a distance ≤ 1.4 kpc. Thus, it is possible that the system could be an IP at a distance of ≤ 1.4 kpc and in that case, the corresponding X-ray luminosity of the system would be $\leq 10^{33} \text{ erg s}^{-1}$. However, it is very unlikely to find a LMXB pulsar at such a low X-ray luminosity. Also it is not very likely that a supergiant is the infrared counterpart of SAX13 as it would lie outside the Galaxy for the given magnitudes. A main sequence early-type star (e.g., B-type) with temperature of 11,000 - 30,000 K and the radius of 3.0 - 7.5 R_\odot would lie at a distance ≤ 8 kpc, indicating SAX13 could be an accreting neutron star high mass X-ray binary pulsar.

However, for the given flux densities, a late-type giant would also be well within the Galaxy at a similar distance.

To further confirm the above argument, we approximated the black-body model to the extinction-free near-infrared fluxes of SAX13 (shown as open circles in Fig 6). Black-body curves for temperature, $T = 20,000$ K and $T = 3,000$ K are shown in Fig 6 as a solid and a dashed-dotted line respectively and are shifted to match the spectral flux density of SAX13 at H wave-band. The solid line clearly indicates that SAX13 is an early-type main-sequence star of temperature $\geq 20,000$ K. For the sake of completeness, the observed fluxes of SAX13 are also shown in the same figure as filled circles.

Based on the above arguments, it is therefore, possible that SAX13 is indeed an accreting neutron star high mass X-ray binary pulsar at a distance of 1.5 - 8.0 kpc. For the observed X-ray flux of SAX13 (Table 4), the luminosity of the system would be 1.2×10^{33} to $3.4 \times 10^{34} \text{ erg s}^{-1}$. Most of the high mass X-ray pulsars (especially Be X-ray pulsars) are transient in nature and have been observed at luminosities varying from 10^{33} to $10^{38} \text{ erg s}^{-1}$. However SAX13 has been persistent for the past 14 years. Thus it is possible that SAX13 is a persistent Be X-ray binary pulsar, similar to X-Persei (La Palombara et al. 2007; Reig et al. 1998). These systems might be part of an unusual class of accreting neutron stars with high mass companions which have long orbital periods (> 30 days) and low eccentricities (e.g., Pfahl et al. 2002). Such long orbital period indicate that tidal circularisation cannot yet have occurred after the supernova explosion that created the neutron star. Therefore, these low eccentricities must be primordial and the supernova explosion could not have been accompanied by a kick to the neutron star (Pfahl et al. 2002).

As suggested above, a late-type giant can also be an infrared counterpart of SAX13, and in that case, SAX13 would be a member of symbiotic X-ray binary pulsars. Symbiotic X-ray binary pulsars are recently identified as a new class of LMXBs, in which a neutron star rotates in a wide orbit around a M-type giant, accretes matter either from the wind of a M giant or via roche lobe overflow (Iben et al. 1996). Symbiotic X-ray binary pulsars are characterized by faint X-ray emission ranging between $\sim 10^{32}$ to $\sim 10^{34} \text{ erg s}^{-1}$, long pulse periods and long spin-up/down phases (Masetti et al. 2007; Corbet et al. 2008). Thus SAX13 could also be a symbiotic X-ray binary pulsar, at a distance ≤ 9 kpc. These systems are expected to be rare, owing to the short duration of both the K/M giant lifetime and the highly unstable mass transfer stage expected for Roche lobe overflow for LMXBs with $P_{\text{orb}} \geq 2$ days (Kalogera et al. 1996).

With the present X-ray and near-infrared observations of SAX13, we are unable to distinguish it to be a high mass accreting X-ray pulsar or the symbiotic X-ray binary pulsar. However, infrared spectroscopic observations would further help to constrain the spectral type of the infrared counterpart of SAX13.

5.2 SAX 1452.8-5949

We detected a faint star in the ESO-NTT images of SAX14, consistent with the *Chandra* error circle, shown in Figure 1. Therefore we identify ‘S1’ as the infrared counterpart of SAX14. Taking $N_H = 1.22 \times 10^{22} \text{ cm}^{-2}$ (Table 4), we cal-

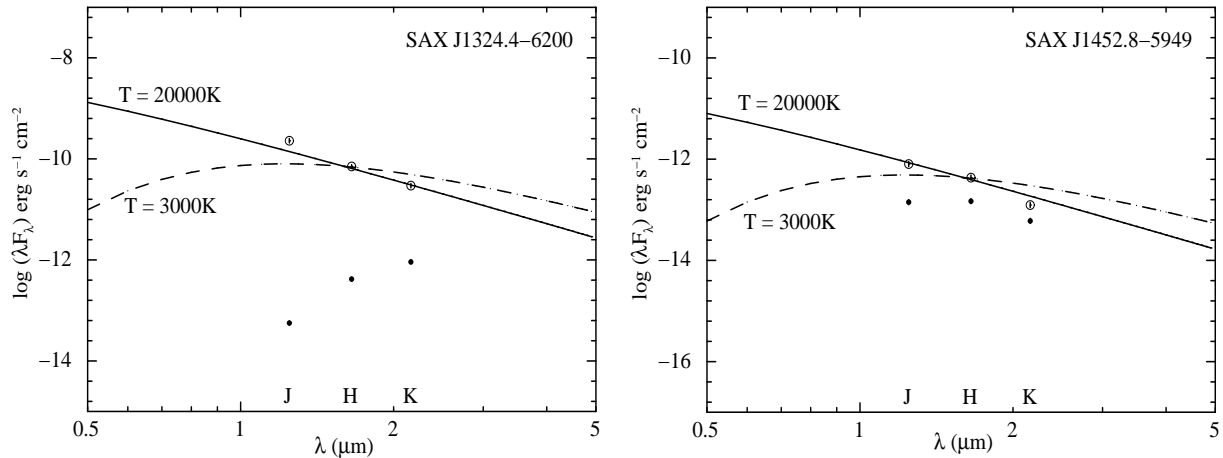


Figure 6. Observed (open circles) and extinction-free (filled circles) spectral energy densities of near-infrared counterpart of SAX1324.4–6200 (*left*) and SAX1452.8–5949 (*right*). The solid line and dashed-dotted line represents black-body model spectral energy density of the star at temperature, $T = 20,000\text{K}$ and $T = 3,000\text{K}$ respectively and are shifted to match the extinction-free spectral energy density of the star at near-infrared H waveband.

culated the dereddened magnitudes of SAX14 to be $J = 16.66 \pm 0.12$ mag, $H = 16.45 \pm 0.12$ mag and $K = 17.15 \pm 0.12$ mag. We calculated the distance of the possible infrared counterpart with the same method used for SAX13 (see §5.1). We can rule out a supergiant, giant or an O/B-type star as the infrared counterpart of SAX14 as, given the observed flux densities, it would lie outside the Galaxy. This rules out the possibility that SAX14 is a HMXB. Only a late spectral type main sequence star (M through A type) can be in the Galaxy, at a distance ≤ 10 kpc. A black-body approximation to the extinction-free near-infrared fluxes of SAX14 indicate that SAX14 would have temperature $< 20,000$ K (Fig 6). However, in case, a part of the X-ray absorption density is local to the X-ray source, we would expect even lesser extinction in near-infrared wavebands and in that case, the temperature of near-infrared counterpart of SAX14 would be much less than 20,000 K. With the above arguments, we can say that SAX14 must be a binary with a low mass companion (LMXB or IP), regardless if there are pulsations or not.

The *XMM-Newton* spectrum of SAX14 is well fitted with a power-law model of photon index 0.83 (Table 4). Both an accreting pulsar and a white dwarf are consistent with the inferred X-ray spectral parameters, so we cannot distinguish from the X-ray spectral information whether SAX14 is a neutron star or an accreting white dwarf. Also we did not detect any strong Fe 6.4 keV line in the X-ray spectra indicates that it is very unlikely that the system is an IP.

No significant pulsations were detected in 0.2 - 12 keV energy band for SAX14 with an upper limit of 15% on the fractional amplitude at 98% confidence level. This result is in contrast with the previous detection made by Oosterbroek et al. (1999) who detected pulsations with a fractional amplitude of $75 \pm 25\%$. To explain this discrepancy we are left with two possibilities: the fractional amplitude of the pulsations decreased or the pulsations observed by Oosterbroek et al. (1999) were spurious. In the later case, SAX14 can be any non pulsating source in the Galaxy, like LMXB, accreting white dwarf, BY Dra, RS CVn or active star, etc.

If on the other hand the detection of pulsations by Oost-

Table 5. Spin-period history of SAX J1324.4-6200

Telescope	Date (UT)	Spin period (s)	References
<i>ASCA</i>	04 Aug 1994	170.35 ± 0.48	a
<i>BeppoSAX</i>	22 Aug 1997	170.84 ± 0.04	a
<i>ASCA</i>	02 Feb 2000	171.25 ± 0.01	b
<i>Swift</i>	30 Dec 2007	172.84 ± 0.1	c
<i>XMM-Newton</i>	11 Jan 2008	172.86 ± 0.02	d

REFERENCES. – (a) Angelini et al. 1998; (b) Lin et al. 2002; (c) Mereghetti et al. 2008; (d) present paper.

erbroek et al. (1999) was real, then the pulse amplitude has to be reduced by a substantial amount. This behavior has been observed in other LMXBs also where the pulsed fraction decreased on the time-scale of days (Her X-1; Ramsay et al. 2002), hours (GX 1+4; Naik et al. 2005) and minutes (4U 1907+09; In’T Zand et al. 1997). Given the large value for the upper limit we obtained, the possibility that SAX14 is a slow pulsating LMXB or an IP is still open.

With all the above arguments, we suggest that SAX14 is not a high mass X-ray binary pulsar. However, the X-ray spectral, timing properties and infrared flux densities suggest to be a low mass companion (LMXB or IP), regardless if there are pulsations or not.

REFERENCES

- Angelini, L., Church, M. J., Parmar, A. N., Balucinska-Church, M., Mineo, T. 1998, *A&A*, 339, 41
 Baykal, A., Inam, C., Alpar, M. A., in ’t Zand, J., Tod, S. 2001, *MNRAS*, 327 1269
 Bildsten, L. et al. 1997, *ApJS*, 113, 367
 Chakrabarty, D. et al. 1997, *ApJ*, 474, 414
 Corbet, R. H. D., Sokoloski, J. L., Mukai, K., Markwardt, C. B., Tueller, J. 2008, *ApJ*, 675, 1424
 Cox, A. N., ed. 2000, *Allen’s Astrophysical Quantities* (4th ed.; New York: AIP)

- Ferrigno, C., Segreto, A., Santangelo, A., Wilms, J., Kreykenbohm, I., Denis, M., Staubert, R. 2007, *A&A*, 462, 995
- Fitzpatrick, E. L. 1999, *PASP*, 111, 63
- Hulleman, F., in 't Zand, J. J. M., Heise, J. 1998, *A&A*, 337, L25
- Iben, I., & Tutukov, A. V. 1996, *ApJS*, 105, 145
- in 't Zand, J., Strohmayer, T., & Baykal, A. 1997, *ApJ*, 479, L47
- Kalogera, V., & Webbink, R. F. 1996, *ApJ*, 458, 301
- La Palombara, N. & Mereghetti, S. 2007, *A&A*, 474, 137
- Lin, X. B., Church, M. J., Nagase, F., & Balucińska-Church, M. 2002, *MNRAS*, 337, 1245
- Lipunov, V. M. 1992, *Astrophysics of neutron stars* (N.Y.: Springer-Verlag) (1992QB843.N4L5713)
- Masetti, N. et al. 2007, *A & A*, 470, 331
- Mason, K. O. 1997, *MNRAS*, 285, 493
- Mereghetti, S., Romano, P., Sidoli, L. 2008, *A&A*, 483, 249
- Misaki, K., Terashima, Y., Kamata, Y., Ishida, M., Kunieda, H., Tawara, Y. 1996, *ApJ*, 470, L53
- Muno M. P. et al. 2004, *ApJ*, 613, 1179
- Naik, S., Paul, B., Callanan, P. J., 2005, *ApJ*, 618, 866
- Norton, A. J., Watson, M. G., King, A. R., 1991, *Lecture Notes in Physics*, vol 385, p155
- Oosterbroek, T. et al. 1999, *A&A*, 351, L33
- Patterson, J. 1994, *PASJ*, 106, 209
- Pfahl, E., Rappaport, S., Podsiadlowski, P., Spruit, H. 2002, *ApJ*, 574, 364
- Predehl, P., Schmitt, J.H.M.M. 1995, *A & A*, 293, 889
- Ramsay, G., Zane, S., Jimenez-Garate, M. A., den Herder, J; Hailey, C. J. 2002, *MNRAS*, 337, 1185
- Reig, P., Roche, P. 1999, *MNRAS*, 306, 100
- Schlegel, D. J., Finkbeiner, D. P., Davis, M. 1998, *ApJ*, 500, 525
- Skrutskie, M. F., et al. 2006, *AJ*, 131, 1163
- Strüder, L. et al., 2001, *A&A*, 365, L18
- Taylor J.H., 1992, *Philosophical Transactions of the Royal Society of London*, 341, 117
- Torii, K., Kinugasa, K., Katayama, K., Tsunemi, H., Yamauchi, S. 1998, *ApJ*, 503, 843
- Turner, M.J.L. et al. 2001, *A&A*, 365, L27
- van den Berg, M., Tagliaferri, G., Belloni, T., Verbunt, F., 2004, *A&A*, 418, 509
- Vaughan, B. A et al. 1994, *ApJ*, 435, 362